Auxiliary Material for EPAPS:

# Observation of a warped helical spin-texture in $Bi_2Se_3$ from circular dichroism angle-resolved photoemission spectroscopy

Y. H. Wang, D. Hsieh, D. Pilon, L. Fu, D. R. Gardner, Y. S. Lee and N. Gedik



## SI I. Materials and Methods

Single crystal $Bi_2Se_3$ (slightly doped with As to improve its cleaving properties) was grown by melting a 10 g stoichiometric mixture of Bi and Se shot with trace amounts of As powder (x=0.00129) in an evacuated quartz tube at 850°C [S1]. After 12 hours at this temperature, the mixture was cooled to 720°C over 2 hours, then slowly cooled to 650°C over 2 days. The batch was annealed at 650°C for 2 days then furnace cooled to room temperature. Samples were checked to be single phase with X-ray diffraction using a Bruker D8 diffractometer with Cu K$\alpha$ radiation ($\lambda = 1.54$ Å) and a two-dimensional area detector. Single crystals were cleaved *in situ* along the (111) plane at room temperature (298 K) and at chamber pressures better than $6 \times 10^{-11}$ torr. The sample was mounted on a goniometer with six degrees of freedom (three angular and three translational), with each angular degree of freedom having 0.04° precision.

Ultrashort laser pulses with center wavelength $\lambda = 800$ nm and a pulse width of 80 fs at full width half maximum were generated from a Ti:Sapph amplifier system with a 5 kHz repetition rate. To convert these pulses to vacuum ultraviolet energy ($\lambda = 200$ nm), we used

fourth harmonic generation via a two stage process, each utilizing $\beta$-barium borate crystals as the nonlinear medium. The first stage frequency triples the tightly focused ultrashort fundamental light through the nonlinear medium and then separates fundamental, second and third harmonic with a series of wave plates and polarizing beam splitters. The third harmonic and fundamental light are recombined into the second stage with well matched time delay. All four frequencies come out of the nonlinear medium and are separated by a prism pair. To generate circularly polarized photons, linearly polarized 200nm light is passed through a variable wave plate orientated at 45° (-45°) from the linear polarization direction to get left (right) circularly polarized light. To check circular polarization purity, the output light from the variable wave plate is reflected back through the variable wave plate and a polarizer (orientated such that it transmits light linearly polarized in the direction of the input light) and into a power meter. The variable wave plate retardance is optimally adjusted such that the power meter records less than 1% of the input power, which corresponds to a better than 99% circular polarization purity.

Photoelectron pulses generated by 200 nm light are collected by a TOF-ARPES spectrometer [S2] in which they are accepted through a circular entrance aperture with opening angle ±22°, guided through a 1 m long flight path by a series of electrostatic lenses, and imaged by a 2D multi-channel plate delay-line detector. The position and arrival time of the photoelectron relative to the laser pulse arrival at the sample determines its energy and 2D momentum. This is very different from a conventional ARPES experiment based on hemispherical analyzers, where only a single 1D cut in 2D momentum space can be measured at a time.

## SI II. Characterization and elimination of false instrumental circular dichroism

It is known that ultra-high-vacuum chamber windows under stress and after bake-out are birefringent and can change the polarization of light. Other optics like mirrors can also cause change in the polarization of light. We characterize the effect of our vacuum chamber window and other optics after the variable wave-plate by following the same procedure that we use for checking the purity of circularly polarized light immediately after the quarter wave-plate. Namely, we shine the circularly polarized light through the window and normally onto the sample. We then reflect the light back through the window and the variable wave plate and

check the polarization through a polarizer. We find that when the window is birefringent or any mirror causes Kerr rotation and/or ellipticity of light, it leads to a false CD pattern containing a $\sin(2\theta)$ component as shown in Fig. S1.

We compensate for the change of the polarization induced by the window by changing the variable wave plate until the reflected light is perpendicularly polarized with respect to the incident light. Only after this compensation is performed do we observe the correct CD patterns under various experimental configurations as is shown in the main text.

## SI III. Calculation of ARPES matrix elements

In this section we present a textbook matrix element calculation [22] for the photoemission intensity from surface states of a general spin-orbit coupled material. We apply this formalism to quantitatively extract the vectorial spin texture of $Bi_2Se_3$, although general features of the spin texture can be directly obtained from the raw data alone.

The microscopic Hamiltonian for an electron in a solid is given by:

$$H = \frac{\vec{P}^2}{2m} + V(\vec{r}) + \frac{\hbar}{4m^2c^2}(\vec{P} \times \vec{\nabla} V) \cdot \vec{s} \tag{1}$$

where $\vec{P}$ is momentum operator, $V(\vec{r})$ is crystal potential due to ions, and $\vec{s}$ is the electron spin. The last term is spin-orbit interaction which comes from relativistic corrections. (Note that $\nabla V$ here is not just the macroscopic electric field near the surface.) Coupling of an electron to an electromagnetic field is obtained via the substitution $\vec{P} \to \vec{P} - e\vec{A}$, where $\vec{A}$ is the photon vector potential, such that to first order in $\vec{A}$:

$$H(\vec{A}) = H - \frac{e}{m}\vec{P} \cdot \vec{A} - \frac{\hbar e}{4m^2c^2}(\vec{\nabla} V \times \vec{s}) \cdot \vec{A} \equiv H - \vec{\mathcal{P}} \cdot \vec{A} \tag{2}$$

In addition to the standard dipole term, $\vec{\mathcal{P}}$ also includes a spin-dependent term arising from spin-orbit coupling. The matrix element between the initial surface states and the final states in the photoemission process is given by

$$M(\vec{k}, f) = \langle f_{\vec{k}} | \, \vec{\mathcal{P}} \cdot \vec{\mathcal{A}} \, | \vec{k} \rangle \tag{3}$$

Here $|\vec{k}\rangle$ labels the 2D surface state at momentum $\vec{k} = (k_x, k_y)$, which is non-degenerate and has a definite spin polarization; $|f_{\vec{k}}\rangle$ labels a final state which must have the same $k_x$ and

$k_y$ as the initial state and have an energy $\hbar\omega$ greater than the initial surface state owing to energy and momentum conservation. The complex quantity $\vec{\mathcal{A}} \equiv \int dt \vec{A}(t) e^{i\omega t}$ is responsible for photon absorption processes. Consider a beam of circularly polarized light incident onto the surface with wavevector in the $xz$ plane, where $x$ is along the $\Gamma K$ direction and $z$ is perpendicular to the surface. The corresponding vector potential is given by

$$\vec{A}(t) = (A_x \sin\omega t, A_y \cos\omega t, A_z \sin\omega t) \tag{4}$$
$$\vec{\mathcal{A}} = (-iA_x, A_y, -iA_z)$$

To calculate the matrix element $M(\vec{k}, f)$ quantitatively requires knowing the microscopic electron wavefunctions and crystal potential near the surface. However, as we now show, the *momentum dependence* of $M(\vec{k}, f)$ near $\vec{k} = 0$ can be obtained analytically without need for such details. This is because in the $\vec{k} \to 0$ limit only the spin polarization $\vec{s}$ depends on momentum $\vec{k}$ in a singular way, whereas all other quantities in (3) are smooth functions of $\vec{k}$ and can therefore be replaced by their values at $\vec{k} = 0$. In particular, the initial state $|\vec{k}\rangle$ is given by

$$|\vec{k}\rangle = u_{\vec{k}} |\phi^i_+\rangle + v_{\vec{k}} |\phi^i_-\rangle \tag{5}$$

where $|\phi^i_\pm\rangle$ denotes the two degenerate surface states at $\vec{k} = 0$ with *total* angular momentum $J^z = L^z + s^z = \pm\frac{1}{2}$. Note that we do *not* need to assume that $|\phi_\pm\rangle$ are $s^z$ eigenstates with 100% spin polarization. More precisely, they are pseudospin eigenstates because spin and orbital degrees of freedom are not independently conserved in a spin-orbit coupled system. Therefore the two component spinor $(u_{\vec{k}}, v_{\vec{k}})$ in reality specifies the spin polarization at momentum $\vec{k}$. The only assumption we make is that the final states $|f_{\vec{k}}\rangle$ have negligible spin splitting at small $\vec{k}$ so that they can be approximated by the two spin degenerate states *at* $\vec{k} = 0$: $|\phi^f_+\rangle$ and $|\phi^f_-\rangle$. This is a very valid assumption because the final states have energies around 6 eV above the surface states so that they are well within the spin-degenerate bulk band continuum. We do *not* need to assume that final states are free electron like plane waves nor that they have zero spin-orbit coupling.

We now calculate the matrix elements between initial states $|\phi^i_\pm\rangle$ and final states $|\phi^f_\pm\rangle$. Because $|\phi^{i,f}_+\rangle$ and $|\phi^{i,f}_-\rangle$ form time reversed partners, it follows from time reversal symmetry

that

$$\langle\phi_+^f|(\mathcal{P}_x+i\mathcal{P}_y)|\phi_-^i\rangle=\Big[\langle\phi_-^f|(\mathcal{P}_x-i\mathcal{P}_y)|\phi_+^i\rangle\Big]^*,$$
$$\langle\phi_+^f|\mathcal{P}_z|\phi_+^i\rangle=-\langle\phi_-^f|\mathcal{P}_z|\phi_-^i\rangle^* \tag{6}$$

Using the mirror reflection symmetry about $yz$ plane

$$M_x:\ x\to -x, |\phi_+\rangle\to i|\phi_-^i\rangle, |\phi_-^f\rangle\to i|\phi_f,\downarrow\rangle, \tag{7}$$

we find

$$\langle\phi_+^f|(\mathcal{P}_x+i\mathcal{P}_y)|\phi_-^i\rangle=-\langle\phi_-^f|(\mathcal{P}_x-i\mathcal{P}_y)|\phi_+^i\rangle,$$
$$\langle\phi_+^f|\mathcal{P}_z|\phi_+^i\rangle=\langle\phi_-^f|\mathcal{P}_z|\phi_-^i\rangle \tag{8}$$

It follows from three-fold rotational symmetry that all other matrix elements of $\mathcal{P}_x\pm i\mathcal{P}_y$ and $\mathcal{P}_z$ vanish. Combining (6) and (8), we obtain

$$\langle\phi_+^f|(\mathcal{P}_x+i\mathcal{P}_y)|\phi_-^i\rangle=-\langle\phi_-^f|(\mathcal{P}_x-i\mathcal{P}_y)|\phi_+^i\rangle\equiv ia,$$
$$\langle\phi_+^f|\mathcal{P}_z|\phi_+^i\rangle=\langle\phi_-^f|\mathcal{P}_z|\phi_-^i\rangle\equiv ib, \tag{9}$$

where $a$ and $b$ are two *real* constants. Substituting (5) and (9) into the (3), we obtain the photoemission transition rate from the matrix element

$$\sum_s|M(\vec{k},s)|^2=a^2\left(|\mathcal{A}_x|^2+|\mathcal{A}_y|^2\right)+b^2|\mathcal{A}_z|^2+a^2\mathrm{Im}\left(\mathcal{A}_x\mathcal{A}_y^*\right)\left(|u_{\vec{k}}|^2-|v_{\vec{k}}|^2\right)$$
$$+2ab\mathrm{Im}\left[\mathcal{A}_x^*\mathcal{A}_z(iv_{\vec{k}}^*u_{\vec{k}}-iu_{\vec{k}}^*v_{\vec{k}})-\mathcal{A}_y^*\mathcal{A}_z(u_{\vec{k}}^*v_{\vec{k}}+v_{\vec{k}}^*u_{\vec{k}})\right] \tag{10}$$

where we have summed over the two degenerate final states $s=\uparrow,\downarrow$. To simplify the above expression, we now introduce a pseudospin Pauli matrix $\sigma^z=\pm1$ to denote the Kramers doublet $|\phi_\pm^i\rangle$. Using the identity $|u_{\vec{k}}|^2-|v_{\vec{k}}|^2=\langle\sigma^z\rangle_{\vec{k}}$, $u_{\vec{k}}^*v_{\vec{k}}+v_{\vec{k}}^*u_{\vec{k}}=\langle\sigma^x\rangle_{\vec{k}}, iv_{\vec{k}}^*u_{\vec{k}}-iu_{\vec{k}}^*v_{\vec{k}}=\langle\sigma^y\rangle_{\vec{k}}$, we find

$$\sum_s|M(\vec{k},s)|^2=I_0+a^2\mathrm{Im}(\mathcal{A}_x\mathcal{A}_y^*)\langle\sigma^z\rangle_{\vec{k}}+2ab\left[\mathrm{Im}(\mathcal{A}_x^*\mathcal{A}_z)\langle\sigma^y\rangle_{\vec{k}}-\mathrm{Im}(\mathcal{A}_y^*\mathcal{A}_z)\langle\sigma^x\rangle_{\vec{k}}\right], \tag{11}$$

where $I_0\equiv a^2\left(|\mathcal{A}_x|^2+|\mathcal{A}_y|^2\right)+b^2|\mathcal{A}_z|^2$ is a $\vec{k}$ independent contribution. Eq.(11) is our main result: it directly relates the photoemission transition rate to the spin polarization of surface states. Note that our derivation is entirely based on symmetry analysis: the right hand side of (11) is the only combination of the vector potential and the spin polarization

which is invariant under time reversal and $C_{3v}$ crystal symmetry. If we change the helicity of light, $A_y \to -A_y$. So the difference in ARPES intensity taken with left and right circularly polarized light is given by

$$\Delta I = a^2 \mathrm{Im}(\mathcal{A}_x \mathcal{A}_y^*)\langle s^z \rangle_{\vec{k}} - 4ab\mathrm{Im}(\mathcal{A}_z \mathcal{A}_y^*)\langle s^x \rangle_{\vec{k}} \tag{12}$$

To measure $\langle s^y \rangle$, we use the fact that measuring $\langle s^y \rangle$ at a particular $k$-point is equivalent to measuring $\langle s^x \rangle$ of that same $k$-point after rotating the sample by 90° about $\hat{z}$.

We note that these matrix elements we calculate for photoemission intensity hold perfectly well in a non-interacting electron picture where the sudden approximation is valid [S4]. These conditions are fully met in our experiment because the band structure of $Bi_2Se_3$ is well modeled neglecting electron correlations [16,17] and the sudden approximation has been shown to be valid when using 6 eV photons [S4].

## SI IV. Method to obtain the in-plane spin deviation angle

In this section, we provide the detailed method of obtaining the in-plane spin deviation angle ($\delta$) from the direction perpendicular to $\vec{k}$ [Fig. 4(b) and (d)]. First we note that in the Dirac regime where the spin texture is rotationally invariant, $\delta I$ is independent of the sample angle $\phi$. Therefore even though $\langle S_x \rangle$ can be independently measured from $\langle S_z \rangle$ by taking sums of $\Delta I$ at different $\phi$ such as $\Delta I(60°) + \Delta I(0°)$ or $\Delta I(90°) + \Delta I(30°)$, this procedure is the same as only measuring $\Delta I$. Both procedures show a $\sin(\theta)$ dependence as is clearly shown in Fig.S4(a).

Outside the Dirac regime, there are two possible effects that can cause $\langle S_x \rangle$ to deviate from being perfectly sinusoidal in $\theta$ as observed in Fig. 4(b). 1) There is a non-uniform out-of-plane canting of the spins around the Fermi contour that modulates the magnitude of the in-plane spin component and 2) the angle between the in-plane spin component and the momentum direction is modulated around the Fermi contour. To figure out which effect is relevant in $Bi_2Se_3$, we study the symmetry properties of these two effects. The combination of $C_{3v}$ crystal symmetry and time-reversal symmetry impose a six-fold rotational symmetry of the in-plane spin component and a three-fold rotational symmetry of the out-of-plane component. Mirror symmetry along the $\Gamma - M$ line dictates that whenever $\theta$ is along $\Gamma - M$

(namely at integer multiples of 60°) then $\langle\vec{S}\rangle$ must be perpendicular to the momentum. Taking these constraints into account allows us to write a general symmetry allowed expression for how $\langle S_x\rangle$ varies with $\theta$

$$\langle S_x\rangle(\theta) = S_0\sqrt{1-[\gamma\sin(3\theta+3\phi)]^2}\times\sin[\theta+\delta\sin(6\theta+6\phi)] \tag{13}$$

where $S_0$ is the total spin, $\gamma \equiv S_z/S_0$, $\phi$ is the angle between $\Gamma - M$ and the in-plane wave vector of the incident photon and the $\sin 3\theta$ dependence of $\langle S_z\rangle$ is confirmed in Fig. 4(a). It is clear from this equation that even though the presence of $\langle S_z\rangle$ does modulate the magnitude of $\langle S_x\rangle$, it can only impose an envelope rather than create sharp kinks in the $\theta$ dependence of $\langle S_x\rangle$ near $\theta = 0°$ as observed by the poor fit to the $\Delta I(90°) + \Delta I(30°)$ trace [Fig. S4(b)] when $\delta$ is set to zero. Another argument against an $\langle S_z\rangle$ origin is that if somehow $\langle S_z\rangle$ were the sole contribution, the fit would imply an out-of-plane canting angle of nearly 45° at $E_F$, which far exceeds theoretical predictions of around 10° [27]. Instead, letting $\delta$ be finite is the only way to explain these kinks. By fitting equation (13) to $\Delta I(90°) + \Delta I(30°)$ at each energy over the entire Dirac cone, we obtain $\delta$ as a function of energy as well as the ratio $\gamma$. Our result shows that the maximum magnitude of $\langle S_z\rangle$ is less than 30% of $S_0$ at 0.4 eV, which corresponds to a much more realistic canting angle of less than 17°.

## SI V. Fitting of $\langle S_z\rangle$ and hexagonal warping

In this section we describe the procedure of fitting results of $k\cdot p$ theory [19] to the data shown in Fig. 4. The magnitude of $\langle S_z\rangle$ as a function of energy along the $\Gamma - K$ direction is described by

$$\langle S_z\rangle^0(E) = 1/\sqrt{1+[k(E)\beta]^{-4}} \tag{14}$$

where $\beta \equiv \sqrt{\lambda/v}$. For $Bi_2Se_3$, the hexagonal distortion of the dispersion is relatively small. Therefore we make the assumption that $k \sim E/v_F$ over the energy range 0 - 0.3 eV. $\langle S_z\rangle^0(E)$ can then be fitted with one free parameter $b \equiv \beta/v_F$. We subsequently extract $\lambda$ by fitting the following $k\cdot p$ result [19] for the shape of the constant energy contour at the Fermi energy ($E_F$)

$$E_F(\theta) = \sqrt{v_F k^2 + \lambda^2 k^6\cos^2(3\theta)} \tag{15}$$

to our measured Fermi surface [Fig. 4(c) inset]. Because the combination of fits to $\langle S_z \rangle^0(E)$ and to $E_F(\theta)$ allows us to extract both $v$ and $v_F$, we can also solve for the correction to the Fermi velocity ($\alpha$) that is also given by $k \cdot p$ theory [19] as

$$v_F = v(1 + \alpha k^2) \tag{16}$$

The obtained values for these parameters are listed in the following table.

| | |
|---|---|
| $E_F$ | 0.3 eV |
| $v_F$ | 3.3 eV Å |
| $v$ | 0.47 eV Å |
| $\lambda$ | 125 eV Å$^3$ |
| $\alpha$ | 743 Å$^2$ |

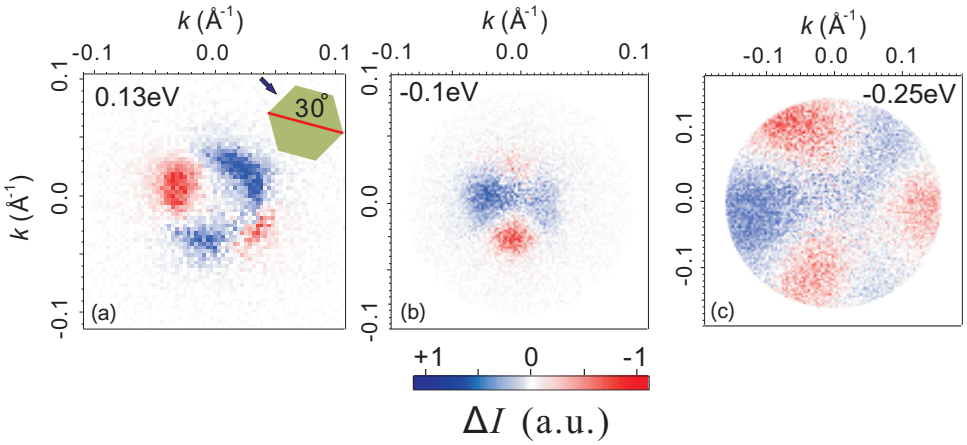


FIG. S1. Constant energy slices at (a)0.13eV (b)−0.1eV and (c)−0.25eV of the CD spectra taken without compensating for vacuum chamber window birefringence. The photon scattering plane is coincident with $\bar{\Gamma}\bar{K}$.

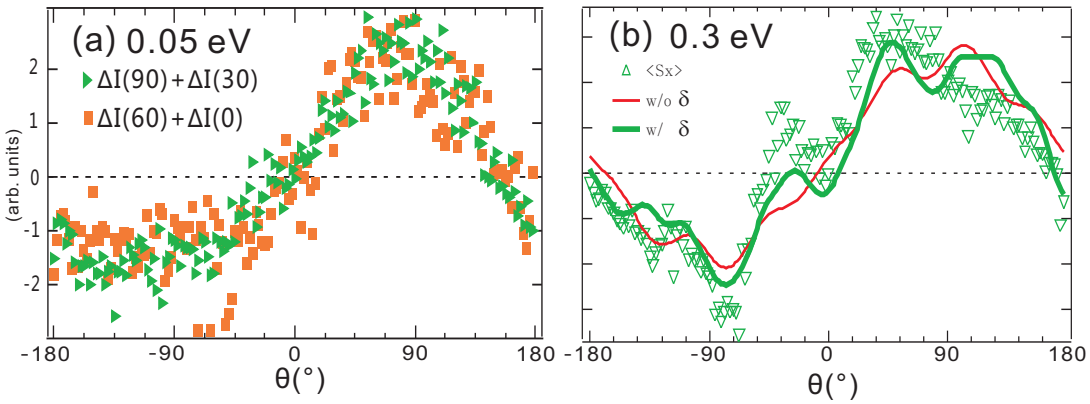


FIG. S2. (a) $\Delta I(\phi = 90°) + \Delta I(\phi = 30°)$ and $\Delta I(\phi = 60°) + \Delta I(\phi = 0°)$ plotted as a function of $\theta$ at an energy of 50 meV. (b) $\Delta I(\phi = 90°) + \Delta I(\phi = 30°)$ at 300 meV together with fits excluding and including $\delta$.

## Supplementary references

**S1.** H. Steinburg, D. R. Gardner, Y. S. Lee, & P. Jarillo-Herrero, *Nano Lett.* **10**, 5032 (2010).

**S2.** We use a commercial ARTOF10K analyzer from VG Scienta.

**S3.** A. Damascelli, *Physica Scripta.* **T109**, 61 (2004).

**S4.** J. D. Koralek, *et al.*, *Phys. Rev. Lett.* **96**, 017005 (2006).